# Analysis of Thickness and Bonding of Multilaminated Films Using One-Dimensional Spectral OCT

M. J. Briones Reyes[#1], G. Rossi Márquez[#2], C.A. Dávalos Saucedo[#3],
[#]Tecnológico Nacional de México: Academia de Investigación, Instituto Tecnológico José Mario Molina Pasquel y Henríquez, Unidad Académica Lagos de Moreno, Jalisco, México
[1]manuel.briones@lagos.tecmm.edu.mx, [2]giovanna.rossi@lagos.tecmm.edu.mx,
[3]cristian.davalos@lagos.tecmm.edu.mx,

***Abstract*—In this work, an optical coherence tomography system is presented. The system was designed to measure the thickness (within 10µm resolution) and give an insight of additional mechanical behavior (bonding) of multi-laminated films. The results demonstrate the feasibility of this kind of system to help provide additional information with contactless and non-invasive techniques, which are significant advantages compared with traditional mechanical systems.**

***Keywords*—optical, analysis, properties, multi-laminated, films.**

## I. Introduction

Multi-layered synthetic films are typically used in packaging engineering to protect the subject from environmental effects. In food packaging, each layer has a unique purpose, such as protecting the sample from oxidation or providing evaporation porousness inside out. In gas-liquid barrier films, producing the right thickness of each coating is vital. If the layer is too thin, the conditions might not be accomplished; in contrast, if the coating is too thick, there will be material waste. The typical physic characteristics that must be examined comprise the thickness and homogeneity of individual and multi-laminated films and contaminations. Traditionally, a vernier caliper or micrometer is used to measure the thickness of the layer. Nevertheless, these instruments yield a variety of errors, such as lower resolution than optical techniques, parallax error, and application of pressure over non-rigid films, among others. The method to achieve this task has to be non-invasive and non-destructive, high-speed, and must show the internal structure of materials.

Low-coherence and coherent-light optical techniques can measure samples' physical, optical, and mechanical properties. Optical coherence tomography (OCT) has been used in a wide variety of fields in medical science besides ophthalmology [1]; for instance, gastroenterology [2], and cardiology [3], among other areas. However, the versatility of OCT allowed it to be applied in engineering areas such as materials science [4] [5], where its measurement range and resolution (ranging from millimeters to micrometers) made it ideal for evaluating the optical and physical characteristics of films or composite materials. OCT uses broadband illumination in the near and mid-range infrared spectrum of light. As in other visible light interferometers, the light from the illumination source is divided by a beam splitter that directs part of the beam towards a reference arm and an object arm containing a mirror and the sample to be analyzed, respectively. Subsequently, the light backscattered by the sample is recombined with the beam reflected by the reference mirror, thus causing interference patterns between the different wavelengths. Finally, the beam is directed towards a spectrometer that varies depending on the type of OCT used.

In temporal OCT, interference patterns are produced by the axial movement of the reference mirror to equalize the optical path difference of the light backscattered by the different layers of the sample. These interference patterns can be observed when the mirror and sample are at equal distance from the beam splitter, with a tolerance equal to the coherence length of the illumination source. Conversely, in spectral OCT, the reference mirror remains static, and the separation of the interference patterns can be resolved with the help of a diffraction grating that angularly separates these patterns before the sensor captures them. The advantages of spectral OCT include high-speed scanning, high sensitivity, and the capability to display two- or three-dimensional reconstructions in real-time. In addition, it has been shown that it is possible to measure the in-plane and out-of-plane strains of samples [6] [7]. This effect allows analyzing not only the physical and optical properties but also the mechanical properties of materials, which is of great interest in materials science.

OCT can give the thickness of coatings [8] [9], or the size and distribution of rivets or filaments. Also, surfaces or impurities can be identified and provide quick signs of the sample's condition, giving researchers valuable evidence.

Moreover, it is feasible to benefit from birefringence for measuring stress and strain using polarization-sensitive OCT [10], to determine the velocity of fluids with Doppler OCT [11], among other properties of materials.

## II. Method

### A. Optical Setup

Figure 1 shows the optical setup, where an 840nm with 40nm bandwidth superluminescent diode (SLD) was used as a light source and an FC/APC optical fiber for beam guidance.

The beam is collimated by a fiber collimator (C), which goes through a 50/50 non-polarizing beam splitter (BC), dividing the beam into the reference and sample beam. Subsequently, the reference beam is focused on the mirror (M)

using a spherical lens (L1 f=100mm). Meanwhile, the sample beam is focused on the sample by another spherical lens (L2 f=100mm). Finally, the interference spectrum is focused on the CCD sensor by L3 (f=250mm) and angularly resolved by a 650 lines/mm diffraction grating (DG).

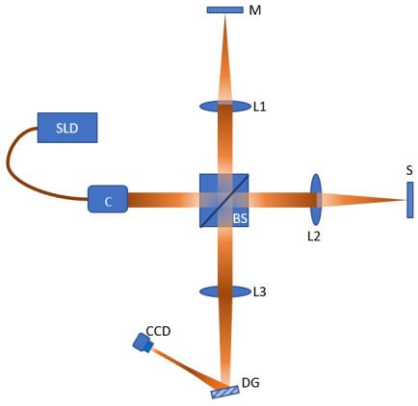


Fig. 1. One-dimensional OCT optical setup.

Since OCT uses a low-coherence light source, it has a coherence length $l_c$ that indicates the distance within each wavelength can interfere with itself [12]:

$$l_c = \frac{1.386}{\pi}\frac{{\lambda_c}^2}{\Delta\lambda} \quad (1)$$

$l_c$ represents the coherence length and is obtained by assuming that the source illumination beam spectrum is Gaussian. $\lambda_c$ is the central wavelength of the illumination source, and $\Delta\lambda$ is its bandwidth.

### B. *Processing*

If the Fourier transform of the bandwidth is obtained, its point spread function (PSF) could be observed. Gaussian profiles of the light source are desirable due to the advantage of their autocorrelation, not presenting side lobes that produce echoes of the structure [13]. However, most manufacturers broad the bandwidth of superluminescent diodes (SLD) by embedding two semiconductors with near spectra, causing lobes to appear in the PSF.

The result of the convolution of the PSF and the sample profile is the combination of interference patterns of the object and reference beams that can be represented as [14]:

$$I(\lambda) = I_R + \sum_{\lambda_{min}}^{\lambda_{max}} I_S(\lambda) + \sum_{\lambda_{min}}^{\lambda_{max}} 2\sqrt{I_R I_S(\lambda)}\cos(\delta(\lambda)) + \sum_{n=\lambda\,\mathrm{min}+1}^{\lambda\,\mathrm{max}} \sum_{m=\lambda\,\mathrm{min}}^{n-1} 2\sqrt{I_S(\lambda_n) I_S(\lambda_m)}\cos(\delta(\lambda_{mn})) \quad (2)$$

Where λ is the wavelength, δ is the phase difference between the wave from the reference and sample beams, *R* and *S* subindex means reference and sample. The first and second terms (reference intensity and sum of the intensities dependent on wavelengths) correspond to the DC term (background noise); the third term denotes the intensity modulated by the interference of the reference beam and the light source's spectrum. While the last one is the modulated intensity resulting from the interference of each wavelength with the others. Applying a frequency transformation and filtering the DC and autocorrelation components, information on the internal structure of the object is obtained:

$$I(\lambda) = \sum_{\lambda_{min}}^{\lambda_{max}} 2\sqrt{I_R * I_S(\lambda)}\, cos(\,\delta(\lambda))) \quad (3)$$

The sample is positioned vertically and fixed over a 1-inch optical round mount on the sample's focused beam plane.

## III. Results

Several tests were made using different films: pectin, protein, and protein-protein. All films were made under the same temperature and humidity conditions, so the only difference between each is the thickness and properties derived from the solutions. Table  summarizes the data in Figures 2 to 5, where a pixel to µm conversion was made according to the depth resolution of the system (1 pixel ≈ 3 µm). Since the 2D image captured by CCD represents 1D information, a mean of 10 rows of the fast Fourier transformation result was made.

TABLE I
SUMMARY OF VOLUMES AND THICKNESS OF PECTIN AND PROTEIN FILMS.

| Solution | Volume | Thickness (µm) | σ (µm) |
|---|---|---|---|
| Pectin | 20ml | 92.3 | 1.9 |
| | 25ml | 99.1 | 2.2 |
| Protein | 30ml | 758.8 | 33.6 |
| | 35ml | 690.4 | 77.2 |

Also, a thickness comparison between random regions of each film was made. The results showed ≈2 µm normal deviation for pectin films and ≈30-80 µm for protein films.

### A. *Pectin*

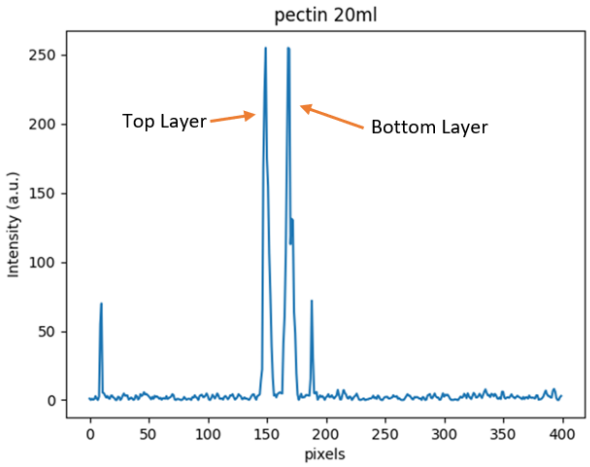


Fig. 2. A-Scan of 20ml pectin film. Peaks indicate the presence of interfaces.

This section shows Pectin films of two thicknesses; both were formed on petry dishes, using 20ml and 25ml of solution.

Figure 2 shows an A-scan (Amplitude scan) of a 20 ml pectin film. The plot shows two peaks of maximum magnitude, which match the interfaces of the film (air-film, film-air). The distance between each peak is proportional to the thickness of the film, as mentioned in Table .

Fig. *3* shows the depth scan of a 25ml pectin film, where a slightly thicker (≈+7 µm) film can be observed compared to the 20ml pectin. It is worth mentioning that all plots' magnitude does not represent the quantitative amount of light captured by the sensor. Still, the maximum sensed for a particular A-Scan, since its *y*-axis is the sample's reflectance and it, directly depends on the angle between the sample and the propagation axis of light.

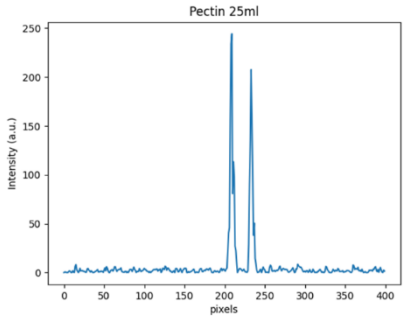


Fig. 3. 25 ml pectin film A-Scan.

## B. *Proteins*

The same procedure of pectin films was performed for protein films. The results indicated that protein film thickness is greater than pectin films for comparable solutions poured in Petri dishes.

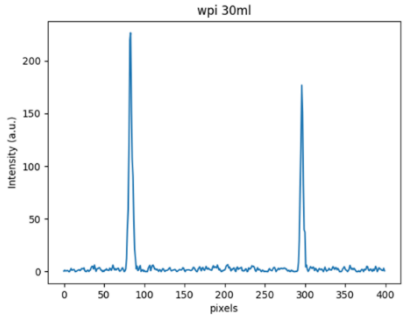


Fig. 4. A-Scan of 30ml protein film.

In Fig. *4* and Fig. *5*, A-Scans of proteic films can be seen. The relative reflectance of each layer (air-film and film-air) indicates the orthogonality of the samples' surface and propagation axis of light, demonstrating a slight non-parallelism among each layer besides the absorption in the irradiation spectrum.

Additionally, a thickness comparison of 30ml and 35ml protein films plots suggests an incongruence since fewer solutions lead to thicker films; nevertheless, Table reveals that the standard deviation of 35ml protein film is greater than 30ml protein film, indicating that 35ml protein film lacks in thickness uniformity than 30ml protein film.

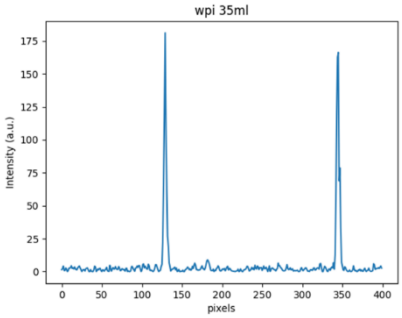


Fig. 5. A-Scan of 35ml protein film.

## C. *Protein-Protein*

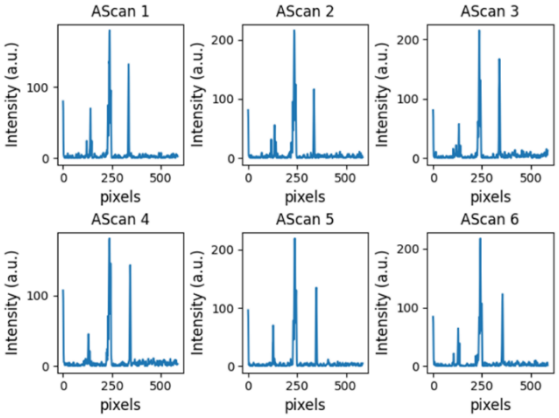


Fig. 6 Series of A-Scans at different points over a multi-laminated protein-protein film.

All previous tests were realized to be demonstrated as a proof of concept. The main goal of this project is to analyze the level of adhesion among other physical properties of multi-layered films.

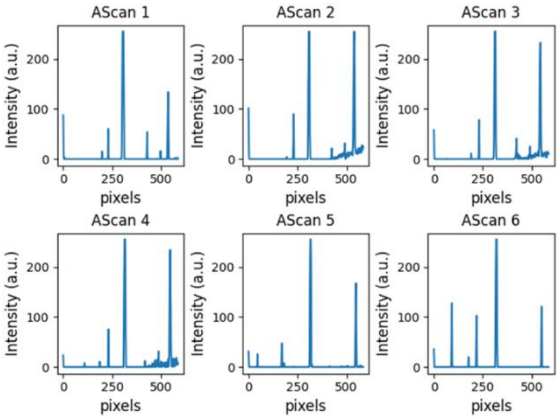


Fig. 7. A-Scans near edges of multi-laminated protein-protein films.

All plots in this section show a series of A-Scans recorded at random sections of one film for each figure. The initial tests

were made using two protein films as those are thicker than pectin films and their ease of manipulation. Fig. *6* exhibits a firm adhesion between films. This test used distilled water as a binding agent and laminated at 40ºC. Whereas in Figure 7, the top and bottom films present unbonded regions (A-Scan 6) corresponding to the edges of the multilaminate film. Finally, Fig. *8* displays a series of A-Scan where an air bubble was trapped inside a multi-laminated film. It can be seen as a gap on each pair of peaks of the top and bottom films.

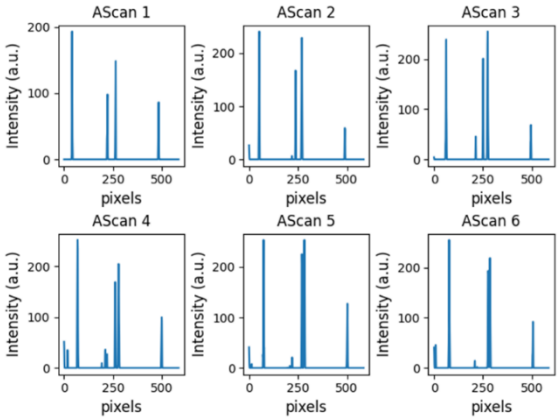


Fig. 8. A-Scans of a multi-laminated film with an air bubble trapped.

## IV. Conclusions and Discussions

This work demonstrates the use and advantages of OCT as a contactless and non-invasive technique to study multi-laminated films. OCT can retrieve the thickness of films and the bonding of multi-laminated films. Since this OCT system works on a single point over the sample, the processing can be executed in real-time (10 fps), and less power is needed to observe the sample's internal structure. Nevertheless, further studies must be done to maximize the information retrieved within a single shot. In addition, a modification of the OCT system is planned to simplify the visualization of defects and physical characteristics of multi-laminated films by allowing reconstruction slices (B-Scans) of the internal structure from A-Scans information. In Fig. *6* through Fig. *8*, a displacement over the depth axis (pixels) is present, indicating the deformation of films. This deformation could be caused by the temperature and pressure exposed in the multilaminate process. Furthermore, the stiffness of multi-laminated films was increased, but not as substantially as desired. In the upcoming stages, the integration of PET films is planned.

## Acknowledgment

The authors are grateful for the facilities granted by the Instituto Tecnológico José Mario Molina Pasquel y Henríquez campus Lagos de Moreno to develop this project and to the Consejo Nacional de Humanidades, Ciencias y Tecnologías (CONAHCYT) for the support and facilities in the development of this project. This research was supported by PRODEP according to grant 31525 assigned to ITJMMPHCA-11.

## References

[1] A. F. Fercher, "Measurement of intraocular distances by backscattering spectral interferometry," *Optical communications*, vol. 117(1-2), pp. 43-48, 1995.

[2] G. J. Tearney, "In vivo endoscopic optical biopsy with optical coherence tomography," *Science*, vol. 276(5321), pp. 2037-2039, 1997.

[3] J. Rogowska, N. A. Patel, J. G. Fujimoto and M. E. Brezinski, "OCT elastography technique for measuring deformation and strain of atherosclerotic tissues," *Heart*, vol. 90(5), pp. 556-562, 2004.

[4] R. J. Young. *Introduction to polymers.* CRC Press, 2011.

[5] J. P. Dunkers, R. S. Parnas, C. G. Zimba, R. C. Peterson, K. M. Flynn, J. G. Fujimoto and B. E. Bouma, "Optical coherence tomography of glass reinforced polymer composites," *Composites Part A: Applied Science and Manufacturing*, vol. 30(2), pp. 139-145, 1999.

[6] M. H. De La-Torre Ibarra, P. D. Ruiz and J. M. Huntley, "Simultaneous measurement of in-plane and out-of plane displacement fields in scattering media using phase-contrast spectral OCT," *Optics Letters*, p. 34(6), pp. 806-808, 2009.

[7] M. H. De La-Torre Ibarra, P. D. Ruiz and J. M. Huntley, "Doble-shot depth-resolved displacement field measurement using phase-contrast spectral optical coherence tomography," *Optics Express*, vol. 14(21), pp.9643-9656, 2006.

[8] M. Gómez Guillén, M. Ihl, V. Bifani, A. Silva and P. Montero, "Edible films made from tuna-fish gelatin with antioxidant extracts of two murta ecotypes leaves", *Food Hydrocolloids*, vol. 21(7), pp. 1133-1143, 2007.

[9] S. González, M. Reyes, G. Márquez, C. Saucedo and M. Martínez, "Caracterización no destructiva de formulación de empaques comestibles usando tomografía de coherencia óptica", *Miscelánea Científica en México*, León , pp. 91, 2020.

[10] M. J. Briones, M. H. De La Torre, F. Mendoza, and J. Pedroza, "Birefringence and deformation measurements in porcine corneas using Fourier domain OCT.," *22nd ICO: Light for the Development*, Puebla, México, 2011.

[11] R. A. Leitgeb, R. M. Werkmeister, C. Blatter, and L. Schmetterer, "Doppler OCT," Progress in retinal and eye research, vol. 41(1), pp. 26-43, 2014.

[12] T. Fuji, M. Miyata, S. Kawato, T. Hattori and H. Nakatsuka, "Linear propagation of light investigated with a white-light Michelson interferometer," *J. Optical Society of America B*, vol. 14(5), pp. 1074-1078, 1997.

[13] D. Huang, Eric A. Swanson, C. P. Lin, J. S. Schuman, W. G. Stinson, W. Chang, M. R. Hee et al., "Optical coherence tomography," *Science*, vol. 254(5035), pp- 1178-1181, 1991.

[14] M. Takeda, H. Ina, and S. Kobayashi, "Fourier-transform method of fringe-pattern analysis for computer-based topography and interferometry," *Journal of Optical Society of America*, vol. 72(1), pp. 156-160, 1982.